Coordinated Management of Electrical Energy in a Steelworks and a Wind Farm

Gonzalo Alonso Orcajo, *Member, IEEE*, Josué Rodríguez Diez, José M. Cano, *Senior Member, IEEE*, Joaquín G. Norniella, Joaquín Francisco Pedrayes González, and Carlos H. Rojas

***Abstract*—This article proposes a coordinated management of electrical energy in a steelworks and a wind farm that are connected to the same distribution network. The suggested solution seeks to improve the efficiency of the hot rolling mill, to reduce greenhouse gas emissions, to minimize the cost of the electrical energy utilized in the manufacture of steel coils, to increase the power system chargeability, and to guarantee power quality. The proposal consists of constituting a virtual plant (comprising the wind farm and the rolling mill) to be managed by a single operator. The approach is mainly focused on the management of the virtual plant reactive power. The algorithm proposed to optimize this reactive power is based on the so-called particle swarm optimization. Three optimization strategies are analyzed: minimization of losses in the distribution network, minimization of the voltage deviation at two of its nodes, and maximization of the displacement factor in both the rolling mill and the wind farm. Energy losses are reduced by up to 20% when adopting the first strategy in comparison to the least efficient case. Voltage variations are kept at less than 1% at both nodes when using the second strategy, whereas deviations between 1% and 5% are obtained when implementing the other two strategies. The study is based on actual measurements and simulation tests.**

***Index Terms*—Hot rolling mill (HRM), particle swarm optimization (PSO), reactive power, steel, virtual plant, wind farm.**

I. Introduction

IMPROVING the energy efficiency of industrial facilities, reducing their emissions of greenhouse gases, and promoting the generation of electrical energy from primary sources of renewable origin are three of the major objectives set by the European Union for the coming years. These objectives must be met while maintaining the competitiveness of the facilities.

Manuscript received December 4, 2021; revised March 12, 2022; accepted March 29, 2022. Date of publication April 7, 2022; date of current version July 19, 2022. Paper 2021-METC-1568.R1, presented at the 2021 IEEE Industry Applications Society Annual Meeting, Vancouver, BC, Canada, Oct. 10–14, and approved for publication in the IEEE Transactions on Industry Applications by the Metal Industry Committee of the IEEE Industry Applications Society. This work was supported by the Research and Development Center of ArcelorMittal (Spain) and by the Spanish Government, MCIN / AEI / FEDER, and the EU, under grants DPI2017-89186-R, PID2021-122704OB-I00 and TED2021-131498B-I00. *(Corresponding author: Gonzalo Alonso Orcajo.)*

Gonzalo Alonso Orcajo, José M. Cano, Joaquín G. Norniella, Joaquín Francisco Pedrayes González, and Carlos H. Rojas are with the Electrical Engineering Department, University of Oviedo, 33204 Gijón, Spain (e-mail: gonzalo@uniovi.es; jmcano@uniovi.es; jgnorniella@uniovi.es; pedrayesjoaquin@uniovi.es; chrojas@uniovi.es).

Josué Rodríguez Diez is with the Basque Country Research Centre, ArcelorMittal, 48910 Sestao, Spain (e-mail: josue.rdgz.diez@gmail.com).

Color versions of one or more figures in this article are available at https://doi.org/10.1109/TIA.2022.3165521.

Digital Object Identifier 10.1109/TIA.2022.3165521

Steel plants and, more specifically, rolling mills are part of the electro-intensive industry. Metallurgical and steel factories came together in the 1970s in Europe. Their high electric power demand forced these factories to be located close to large generation centers, where it was possible to obtain good prices per kWh and where thermoelectric power plants prevail nowadays, particularly those based on the use of coal.

The directives of the European Union about environmental matters and particularly in relation to greenhouse gas emissions will necessarily force the reconversion of both sectors in the immediate future. Coal thermal power plants will be required to incorporate desulfurization, denitrification, and CO_2 capture systems into their production lines to avoid closure. As a matter of fact, various countries have already announced the closure of part of their coal-based plants in the short-term. Consequently, renewable generation is likely to be promoted to restore part of the dismantled power capacity. The already existent high-power transport networks, originally designed to cover thermoelectric generation, will favor the power restitution to a certain extent. However, the price per kWh might become more expensive under these circumstances, which could lead to the relocation of metallurgical and steel plants to countries with less demanding environmental directives and cheaper energy prices.

In order to consolidate the steel industry in the current production centers, it is necessary to design strategies aimed at reducing the costs of electric energy and at guaranteeing power quality while meeting the objectives in terms of energy and climate change or the profitability of the plants.

Exhorted by the EU [1], some steelmakers have started taking measures to reduce the emissions of CO_2 from their manufacturing plants over the coming decades. These measures are primarily aimed at curtailing the production of steel from coal-fired blast furnaces while simultaneously boosting that of direct reduced iron by using renewable energy sources such as green hydrogen. Moreover, the integration of renewable energy-based electricity generators into the plants and the increase in the use of scrap in electric arc furnaces are likewise contemplated, the target being to stimulate the consumption of electricity involving low or zero greenhouse gas emissions, e.g., that from solar or wind power sources. In this article, a steelworks whose electric distribution network includes a wind farm is considered.

The opportunities offered by the coordinated operation of consumption and generation centers have been analyzed by other authors in the context of smart grids [2]–[4]. Such grids integrate energy consumption, storage, and renewable-based generation

systems. Virtual power plants are one of the clearest examples of a joint and coordinated operation of several agents with common interests, both technical and economic [5]–[9]. The efficient management of reactive power is one of the capabilities of these virtual plants, where different agents collaborate by means of coordinated actions according to their rated powers and their particular operating conditions.

The algorithms for reactive power management and optimization in power systems are based on conventional and advanced procedures [10]. The former are based on linear [11] and nonlinear programming [12]. The latter can be based, for example, on neural networks [13], genetic algorithms [14], or heuristic and metaheuristic methods [15]. The particle swarm optimization (PSO) belongs to the group of metaheuristic methods [16], [17]. In this article, a widely used and suitable PSO-based algorithm is considered, as will be discussed. More specifically, this article proposes the joint, coordinated, and collaborative exploitation of a hot rolling mill (HRM) and a wind farm. The solution primarily seeks to improve the efficiency of the rolling mill, to reduce greenhouse gas emissions, to decrease the cost of electrical energy, to increase the power system chargeability, and to guarantee power quality. The proposal consists of developing a virtual plant including the wind farm and the rolling mill. This virtual plant will be managed by an operator [18] that must meet the production objectives by observing the economic benefits that can be provided by the electricity market, the possible energy production according to weather forecasts and the services that can be offered to the distribution network. In order to promote this proposal, the electricity market operator could take such services into account in the daily management of the power system and, therefore, remunerate them in a regulated manner.

The virtual plant will be controlled by only one agent to buy and sell active power in agreement with the daily market in each supply zone, to program the daily rolling campaigns according to demand management criteria, to offer services related to reactive power injection, and to optimize the internal reactive power flows according to multiple-criteria target functions that can take into account parameters such as the reduction of distribution losses or the control of voltage stability and variations.

The rest of the article is organized as follows. In Section II, the rolling mill plant and its associated distribution network are presented. The characteristics of the wind farm are briefly reported in Section III. Section IV describes several of the main objectives of the virtual plant. The reactive power management strategy and the objective functions that can be addressed by the optimization algorithm are included in Section V. This algorithm, based on PSO, is described in Section VI. Several case studies are presented in Section VII. In Section VIII the proposal is validated, and the advantages are demonstrated. Finally, the conclusions of this study are gathered in Section VIII.

II. Steel Plant and Distribution Network

The original HRM considered in this study is a classic plant built in the 1980s and whose main electrical load is a roughing and finishing train. The roughing mill (RM) has two main drives (upper and lower). The finishing mill (FM) comprises six rolling

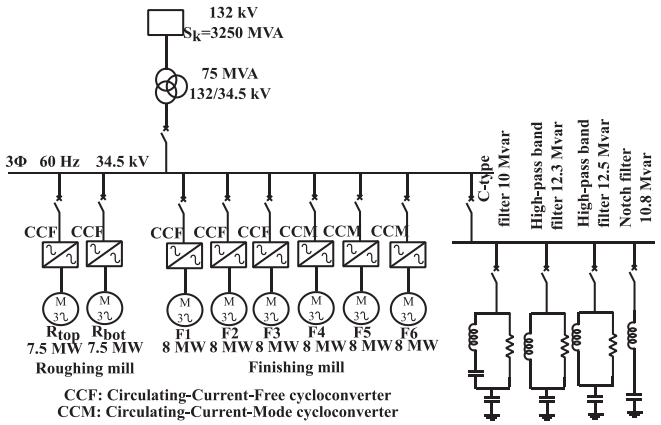

Fig. 1. Single-line diagram of the original plant.

stands. The drives are based on 12-pulse cycloconverters capable of controlling the synchronous motors that drive the rolls through a gear train. This topology also includes a passive filtering system to limit the injection of harmonics into the distribution network and to compensate for reactive power (see Fig. 1).

The average electric energy consumption in the hot-rolling operation is between 70 and 80 kWh per ton of produced steel coil. Power quality is also of great importance because steel plants, as large consumers, can affect the distribution network greatly and are particularly sensitive to disturbances. Rolling mill campaigns involve 20–30 slabs per hour and approximately 470–530 slabs per day. Each slab can weigh up to 22–26 tons; therefore, the daily and annual demand in a HRM can reach up to 1 and 365 GWh respectively, which is why proposals aimed at improving their energy efficiency offer a great opportunity for considerable savings [19].

In order to improve the reactive power management, a 15-MVA STATCOM is connected to the point of common coupling of the drives and the passive filtering system. The rated power of the STATCOM is selected based on three main objectives. First, to ensure a backup for the passive filtering system. Because the highest rated power out of the four branches of this system is 12.5 Mvar, the 15-MVA STATCOM can provide the corresponding reactive power in case of one of the branches going out of service. This backup functionality prevents unscheduled shutdowns in the rolling mill, which cause huge economic and production losses. Second, to provide support for rapid voltage variations in order to comply with regulatory constraints. Third, to guarantee a reasonable amortization period (which results in less than 3 years). The STATCOM is compatible with other future enhancements of the plant, including a renewal of the rolling stands that can also provide support for reactive power management. This is why the minimum rated power has been selected.

A new stage of the plant renewal consists in the incorporation of a wind farm into the 132-kV distribution network that feeds the steel plant, including the rolling mill. The analyzed rolling campaigns are based on real records of an actual rolling mill. Figs. 2 and 3 show the evolution of the active and reactive power demand of the hot rolling mill when ten slabs are rolled.

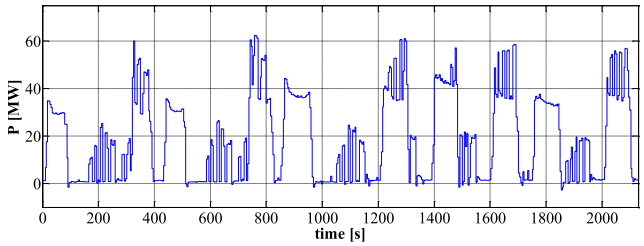

Fig. 2. Active power demand of the hot rolling mill.

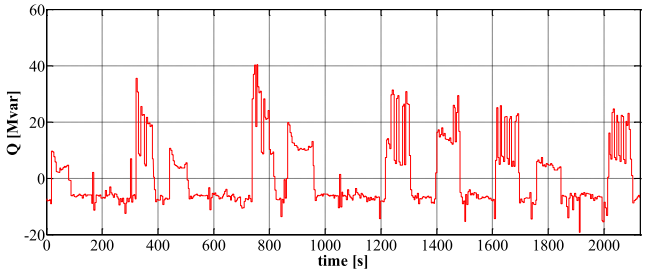

Fig. 3. Reactive power demand of the hot rolling mill.

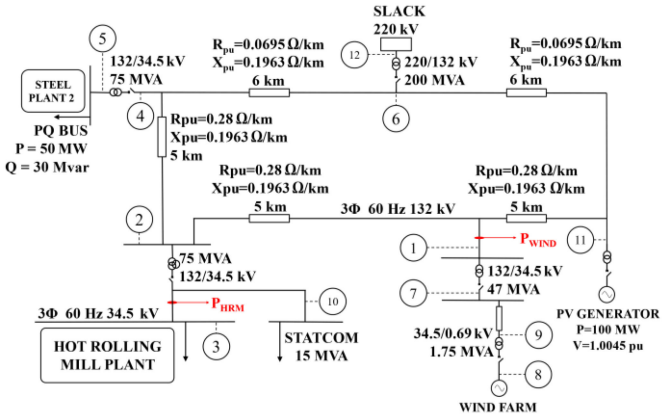

Fig. 4. Single-line diagram: nodes under study.

The rolling mill, the wind farm, and other installations that are part of the steel plant are connected to a 132-kV distribution network (see Fig. 4). The power generation system consists of the wind farm and a 115-MVA plant for the recovery of the waste gases generated both in the blast furnaces during the pig iron production and in the coke batteries. This plant is based on synchronous generators driven by gas turbines. The consumption of the other installations of the steel plant is represented by their active and reactive power flows, which have been assumed to be constant (50 MW and 30 Mvar) in order to focus on the other consumption nodes. The 220-kV transmission network is connected to one of the nodes of the ring distribution grid by means of a 132/220 kV transformer. Tables I and II indicate the main parameters of transformers and cables.

TABLE I
TRANSFORMER PARAMETERS

Transformer	1-Wind	2-Steel	3-HRM	4-Wind	5-Slack
Sn [MVA]	20 x 1.75	75	75	47	200
U1/U2 [kV]	34.5/0.69	132/34.5	132/34.5	132/34.5	220/132
ε_{Rcc}; ε_{Xcc} [%]	1; 5	1; 7.66	1; 7.66	0.53; 16	1; 15
Rm; Xm [pu]	500; inf	500; 500	500; 500	500; 500	500; 500

TABLE II
ELECTRICAL PROPERTIES OF CABLES AT 132 KV

Cable	Nodes	Conductor	s [mm^2]	Ampacity [A]
C1	1-2; 2-4; 1-11	Al	1 x 400	605
C2	4-6;11-6	Cu	1 x 500	1,035

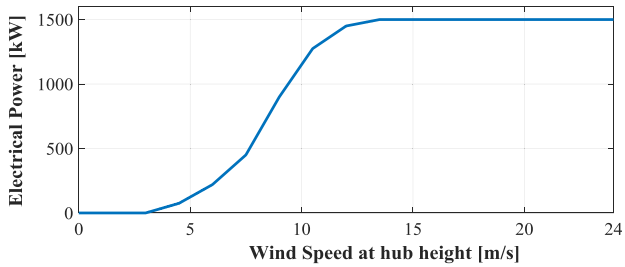

Fig. 5. Wind turbine power curve.

III. WIND FARM

The planned wind farm consists of 20 wind turbines with a rated power of 1.5 MW each (i.e., a total installed capacity of 30 MW) and whose technical data are similar to those of commercial systems [20]. Wind turbine power curve is shown in Fig. 5. The turbines are based on a doubly fed induction generator (DFIG) able to control the active and reactive power flow. The average wind speed at the selected location is assumed to be 7.5 m/s at hub height. Under these conditions and considering a cumulative Weibull distribution of wind duration, each turbine is assumed to generate up to 3.8 GWh/year, which means an annual production of the farm of $20 \cdot 3.8 = 76$ GWh (i.e., a capacity factor of 28.9%). This amount of energy, coming exclusively from renewable sources, would cover 20.8% of the annual demand of the rolling mill. This fact is pivotal to the selection of the rated power of the wind farm. The expected annual generation covers over 20% of the energy demanded by the rolling mill for an overall installed capacity of 30 MW at the considered location, thus complying with the 20% of energy obtained from renewable sources that the EU has set as a key target in recent years. The wind farm provides the plant with active energy generated with low greenhouse gas emissions (GHG) and conditioned by the daily wind speed profile. For a large part of its period of operation, the farm can utilize a reserve to supply capacitive or inductive reactive power depending on the needs.

That reserve can be provided partly by the stator of the induction generator and partly by the converter connected to

TABLE III
ECONOMICAL ANALYSIS

	Low cost scenario	Medium cost scenario
Total cost of investment:	**40M$**	**40M$**
Annual energy generation	76,000 MWh	76,000 MWh
Annual losses	1%	1%
Energy price	50 $/MWh	60 $/MWh
Increase in energy prices	1%/year	1%/year
Savings in CO_2 emissions	----------	0.355 t/MWh
CO_2 price	----------	50 $/t
Amortization period	20 years	20 years
Annual amortisation:	2M$	2M$
Profit tax:	25%	25%
Cost of O&M	20,000 $/MW	20,000 $/MW
Annual O&M cost change:	2%	2%
Discount rate:	3%	3%

TABLE IV
FINANCIAL TOOLS

Simple Payback	13 years	8 years
NPV	3 M$	26.5 M$
IRR	4%	9%

the network. The grid side converter (GSC), which normally manages between 20% and 30% of the nominal power of the wind turbine, can be oversized for the power reserve to be greater. This reserve can be used to control the reactive power and also the injection of harmonics, the GSC thus playing the role of an active filter [21], [22]. At present, a number of wind farms exist either nearby or on the grounds of various steelworks. The coordinated operation of the farm and the steelworks enables collaborative agreements [23].

A. *Economical Analysis*

The feasibility of the wind farm can be estimated by means of an economic analysis and of the calculation of the simple payback, the net present value (NPV), and the internal rate of return (IRR) to determine the financial benefit of investing [24], [25]. Tables III and IV summarize the involved calculations.

The economic analysis is performed under two scenarios. In the first one, "*low cost scenario,*" a low energy price is considered and the economic benefit of saving CO_2 emissions is not taken into account. In the second one, "*medium cost scenario,*" the increase in energy price and the mentioned benefit are observed. In this regard, CO_2 emission allowance (European Union Allowance, EUA) costs have risen considerably over the last years [26]. The wind farm can be amortized in a reasonable period in both cases, even when considering a scenario of further energy price containment.

IV. VIRTUAL PLANT

The main targets of the virtual plant are as follows:

1) Coordinated management of the energy demand.
2) Significant reduction of GHG emissions.
3) Lessening of energy dependence.
4) Improvement in the voltage profile.
5) Decrease in losses.
6) Control of reactive power.
7) Voltage stability.

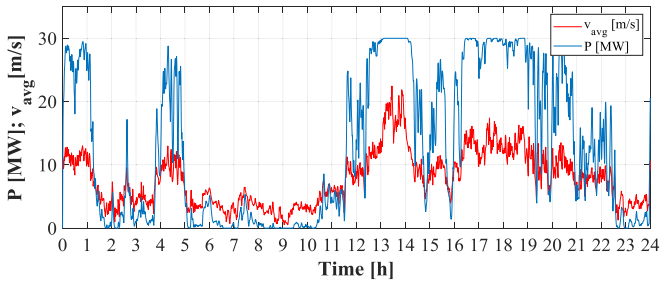

Fig. 6. Average wind speed at 80 m height. Data provided by the National Renewable Energy Laboratory. Date: 03/02/2021 [28].

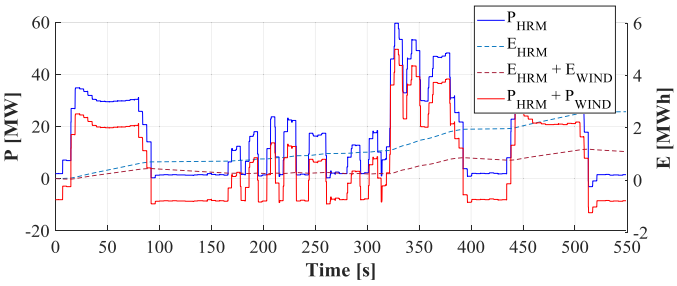

Fig. 7. Active power and energy demand in presence or absence of the wind farm.

8) Control of harmonics.
9) Enhancement of the response under voltage sags.
10) Improvement in the power network reliability.

A. *Coordinated Management of Electrical demand*

The electric power production of the wind farm depends mainly on the average wind velocity and the power–speed curve of its turbines. This production can cover part of the demand of the rolling plant, thus reducing the active power distributed by the 132-kV network, the voltage drop at the PCC and the losses upstream this point.

The average wind speed determines the active power production of the farm and depends, among many other factors, on the local time and season. There are various applications that enable a reliable forecast of the hourly average wind speed between 8 and 10 h in advance [27]. The power produced by a wind farm along with the average daily wind speed is exampled in Fig. 6. As can be seen, the farm operates at rated power (30 MW) between 13:00 and 14:00, while barely 1 MW are supplied from 9:00 to 10:00.

Assuming that the wind farm generates 10 MW under a capacity factor of 0.333 (0.5 MW per turbine, 20 generators), a comparison of the power demanded by the installation in presence or absence of the wind farm can be seen in Fig. 7. The difference in the energy demanded by the installation under the two operating conditions is 1,761 kWh over the 550 s considered rolling profile. The positive impact of the joint operation of the HRM and the wind farm on the active energy consumption is evident.

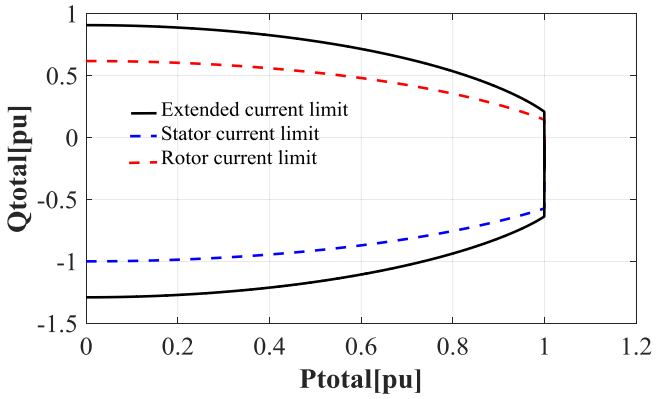

Fig. 8. Reactive power injection limits according to active power supply.

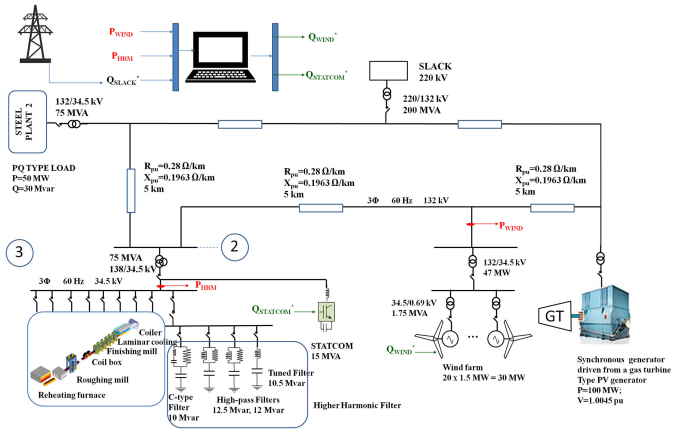

Fig. 9. Diagram of the ring distribution network under study.

The rolling campaigns can be organized seeking for the simultaneity of the generation of energy by the wind farm and the demand of active power while honoring the production criteria of the plant.

B. Emissions of Greenhouse Gases

The CO_2 emissions per kWh are a function of the primary source used by the generation power station. Accordingly, 0.961 kg of CO_2 per kWh are emitted by a coal thermal plant; 0.651 kg of CO_2 per kWh by a fuel-gas plant; 0.372 kg of CO_2 per kWh by a combined cycle natural gas plant, and 0.006 kg of CO_2 per kWh by a wind farm. The emissions of the Spanish electricity mix were estimated at 0.341 kg of CO_2 per kWh in 2018 [29].

The expected reduction in CO_2 emissions in incorporating the wind farm is 25 460 ton per year when compared to the emissions from the energy mix, and 72 580 ton per year with respect to those from a generation system solely based on coal thermal power plants.

C. Control of Wind Farm Reactive Power

The capability of the wind farm to control the reactive power is determined by that of its turbines [30], [31]. Accordingly, the reactive power manageable by the DFIG stator depends on both the active power transferred to the grid and the rated current of the stator itself. It also depends on the rotor rated current and voltage, given that the stator injection of active and reactive power is controlled through the *d–q* components of the rotor current. This control depends, in turn, on the voltage applied by the converter connected to the rotor. Moreover, the injection of reactive power from the GSC is limited by both the rated power of the converter itself and the active power transferred to the grid by the rotor.

Previous works have concluded that the limiting variable as for the injection of reactive power from the DFIG is normally the rotor current whereas the stator current is that for the reactive power demand. The rotor voltage only has influence at high slips. Fig. 8 proves these statements correct by showing the power injection capability of the analyzed wind turbines. The injection of reactive power from the wind farm enables the fulfillment of the network operator needs as for the control of the PCC voltage and the virtual plant displacement factor, as well as for the support against potential voltage sags while avoiding the overload of the wind turbines and the shutdown of the rolling stands.

V. Reactive Power Management System

Reactive power management was mainly handled by large generators in traditional power systems. Nowadays, the increasing proliferation of distributed generation offers the opportunity to decentralize both the active and the reactive power management. In the specific context of industrial production plants, the incorporation of distributed generation systems can improve their operating conditions and bring economic benefits. As for the former, voltage variations at the PCC are controlled, as is the reactive power, which reduces losses and the loading of lines, transformers and protections, and gives support to overcome voltage sags without leading to interruptions in production cycles. As for the latter, the transmission system operator offers a reactive power injection/consumption service able to bring economic benefits to the plant. One of the main objectives of our approach is to ensure that the HRM and the wind farm are managed collaboratively and jointly. Fig. 9 shows the distribution network under study including the main generation and consumption installations.

Once the strategies for managing the active power demand are set, attention must be paid to the optimal management of reactive power. In this case, the goal is to define the most suitable optimization algorithm to set, in real time, the reactive power references for the wind farm generators and the STATCOM connected at the PCC. These references are strongly influenced by the technical constraints of the equipment (wind conditions, nominal power of the wind turbines and the STATCOM, etc.). Moreover, they also depend on the operating conditions of the grid, i.e., the reactive power setpoint at the PCC according to the system operator directives, the existing regulations, and the technical constraints of the distribution grid itself (line current limitations, protections response, voltage stability and variation, etc.).

In general, the presence of numerous dispatchable units guarantees that there are sufficient degrees of freedom to meet the network optimization objectives once the above restrictions are met. This optimization process can address individual objectives or several targets by weighing them appropriately in multi-objective functions, among which the following are assessed:

1) Minimization of losses in the distribution network. This objective involves minimizing the following function:

$$P_{\text{losses}} = \sum_{k} G_k\,(i,j)\,\left[V_i^2 + V_j^2 - 2V_iV_j\cos\left(\delta_i - \delta_j\right)\right] \tag{1}$$

where V_i (and V_j) and δ_i (and δ_j) represent, respectively, the modulus and phase of the voltage at node *i* (and *j*), and G_k, the conductance of line *k* (connecting nodes *i* and *j*).

2) Minimization of the penalty for power factors beyond the admissible range. Spanish regulations concerning energy production from renewable sources set a mandatory power factor between 0.98 capacitive and 0.98 inductive at the PCC [26]. These guidelines may be temporarily modified by the system operator according to the needs of the network and may even respond to the tracking of a voltage reference at a specific node [32].

3) Minimization of the voltage deviation at the nodes of the internal network of the virtual plant, which is usually expressed through factor $\text{VD} = \sum_i |V_i - V_i^*|$, where V_i^* is the voltage assigned to node *i*. The participation in the transmission grid voltage control is remunerated in accordance with the existing guidelines in each country. In Spain, the system operator gives generators in charge of controlling node voltages priority for dispatching purposes, which also provides an economic benefit.

VI. Particle Swarm Optimization

Although reactive power optimization problems are nowadays profusely studied in the literature, our approach aims at responding to several challenges that arise in the application under study. For instance, these optimization problems are traditionally solved by using capacitor banks where automatic power factor regulators must operate with low sensitivities in order not to overload the relays in charge of connections/disconnections, the response times resulting in a range between a few seconds and several minutes [33]. However, the reactive power references sent to the various dispatchable elements in the virtual plant must be updated in a few seconds to maximize the positive impact of this solution. Therefore, heuristic methods (which, although quasi-optimal, are extremely robust) are utilized.

The specific method to be used is the so-called PSO [34]–[36]. The PSO is a metaheuristic optimization strategy based on populations and aimed at finding global minima or maxima. More specifically, population-based metaheuristic methods consist of calculating the trajectory followed by a population of individuals at each iteration to find a quasi-optimal solution from the evolution of a set of points in space. These methods are inspired by the behavior of flocks of birds, schools of fish, or swarms of insects, in which the movement of each individual as for direction, speed, acceleration, etc., is the result of combining their particular decisions and the conduct of the rest. PSO algorithms aimed at maximizing or minimizing a function with one or multiple variables usually take the following steps:

1) creation of an initial swarm of n random particles;
2) evaluation of the objective function for each particle;
3) calculation of the movement of each particle and subsequent update of their position and velocity;
4) verification of stopping conditions and, if not met, return to step 2).

The proposed PSO-based algorithm consists of the following specific steps.

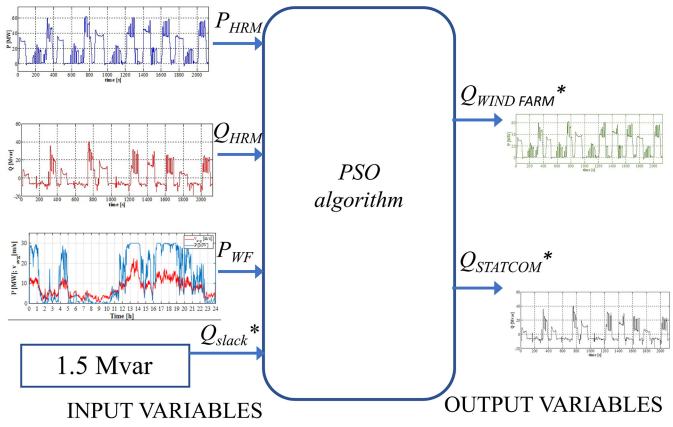

Fig. 10. Input and output variables of the algorithm.

Step 1: Voltages required at each node are set. The nodes are denoted *i* and *j*.

Step 2: Restrictions on the reactive power injected/absorbed by the wind farm and the STATCOM are fixed according to the particular operating conditions.

Step 3: The most representative impedances of transformers and distribution network lines are identified.

Step 4: Elements of the admittance $Y_{i,j}$, susceptance $B_{i,j}$, and conductance $G_{i,j}$ matrices are calculated.

Step 5: Characteristic power values at the PQ buses and the PV bus are identified. Net injected power values are calculated. The algorithm input data (active P_{HRM}, and reactive Q_{HRM}, power of the HRM, and active power of the wind farm P_{WF}) are updated every 10 ms. A schematic in this regard is shown in Fig. 10.

Step 6: The PSO-based optimization algorithm is run. The utilized number of particles (*Np*) is 50 and the expected iterations are 150. The optimization is conducted by acting on two variables, namely the reactive power managed by the wind farm Q_W, and that handled by the STATCOM Q_S. Therefore, the algorithm dimension is 2. Limits to the position of the particles are defined: in the case of the wind farm, according to the generated active power; in the case of the STATCOM, with regard to its nominal power (15 MVA). Inertia weight, $w = 0.729$, cognitive weight, $c1 = 1.49445$, and social weight, $c2 = 1.49445$, are defined.

Step 7: Several matrices are defined: particle swarm position $X_{i,h,}$ (2), particle velocity $V_{i,h,}$ (3), best positions, best values of each particle $p_{\text{best } i,h}$ (4), Jacobian including initial values, and global best values $G_{\text{best},i}$ (5). Moreover, index h is the particle order and varies between 1 and the particle number N_p

$$\begin{bmatrix} X_{1,h} \\ X_{2,h} \end{bmatrix} = \begin{bmatrix} X_{11} \ \dots \ X_{1,Np} \\ X_{21} \ \dots \ X_{2,Np} \end{bmatrix} \tag{2}$$

$$\begin{bmatrix} V_{1,h} \\ V_{2,h} \end{bmatrix} = \begin{bmatrix} V_{11} \ \dots \ V_{1,Np} \\ V_{21} \ \dots \ V_{2,Np} \end{bmatrix} \tag{3}$$

$$\begin{bmatrix} p_{\text{best}1,h} \\ p_{\text{best}2,h} \end{bmatrix} = \begin{bmatrix} X_{\text{best}11} \ \dots \ X_{\text{best}1,N_p} \\ X_{\text{best}21} \ \dots \ X_{\text{best}2,N_p} \end{bmatrix} \tag{4}$$

$$\begin{bmatrix} G_{\text{best}1} \\ G_{\text{best}2} \end{bmatrix}. \tag{5}$$

Step 8: The references for the reactive power of the wind farm Q_W, and STATCOM $Q_{STAT,}$ are established. Reactive power values are assigned to nodes 8 (6) and 10 (7) (see Fig. 4) according to the position of the corresponding particle

$$Q_{W,h} = X_{1,h} \cdot S_{\text{base}} \tag{6}$$

$$Q_{\text{STAT},h} = X_{2,h} \cdot S_{\text{base}}. \tag{7}$$

Step 9: The load flow is solved by using the Newton Raphson's method for the modulus V, and argument θ, of the node voltages to be calculated [(8) and (9)]. First, the node voltages are initialized at 1 p.u. and 0 rad. The voltage at the PV node is set to 1.0045 p.u. Second, the reactive power at the slack bus and at the PV node is obtained to calculate the Jacobian matrix. Third, extended submatrices H, L, M, and N are calculated [(10)–(13)]. Fourth, power mismatches (ΔP and ΔQ) are calculated and compared with a power flow convergence threshold of 10^{-6}. When both power mismatches are lower than this threshold, the Newton-Raphson's algorithm is stopped

$$\begin{bmatrix} H & N \\ M & L \end{bmatrix}^k \cdot \begin{bmatrix} \Delta\theta \\ \Delta V/V \end{bmatrix}^k = \begin{bmatrix} \Delta P \\ \Delta Q \end{bmatrix}^k \tag{8}$$

$$\begin{bmatrix} \theta \\ V \end{bmatrix}^{k+1} = \begin{bmatrix} \theta \\ V \end{bmatrix}^k + \begin{bmatrix} \Delta\theta \\ \Delta V \end{bmatrix}^k \tag{9}$$

$$\text{for } i \neq j: \ H_{ij} = L_{ij}$$

$$= V_i \cdot V_j \cdot (G_{ij} \cdot \sin\theta_{ij} - B_{ij} \cdot \cos\theta_{ij}) \tag{10}$$

$$N_{ij} = -M_{ij} = V_i \cdot V_j \cdot (G_{ij} \cdot \cos\theta_{ij} + B_{ij} \cdot \sin\theta_{ij}) \tag{11}$$

$$for \ i = j: \ H_{ii} = -Q_i - B_{ii} \cdot V_i^2; \ L_{ii} = Q_i - B_{ii} \cdot V_i^2 \tag{12}$$

$$N_{ii} = P_i \ + G_{ii} \cdot V_i^2; \ M_{ii} = P_i \ - G_{ii} \cdot V_i^2. \tag{13}$$

Step 10: Different cost functions are evaluated depending on the selected objective. Therefore, cost functions associated with

1) voltage variations at nodes 3 and 8,
2) losses in the distribution network, or
3) the displacement factor at the PCC of the wind farm and the HRM are assessed.

In the first two cases, the discrepancy between the reactive power injected into the slack bus, Q_{slack}, (14) and that set as a reference, $Q_{\text{slack\_ref}}$, is calculated

$$Q_{\text{slack}} = \text{Imag}\left(V\,(12) \times I^*_{12\_6}\right). \tag{14}$$

The target voltages for nodes 3 and 8 would be $V_{\text{HRM\_OBJ}}$ and V_{W_OBJ} (15). The cost functions, cost_1, cost_2 and cost_U, associated with the objective of minimizing voltage variations are indicated in (16)–(18). K_1 and K_2 are weighting coefficients

$$V_{\text{HRM\_OBJ}} = 1.0 \text{ p.u.}; \ \ V_{W\_\text{OBJ}} = 1.05 \text{ p.u.} \tag{15}$$

$$\text{cost}_1 = |V\,(3) - V_{\text{HRM\_OBJ}}| + |V\,(8) - V_{W\_\text{OBJ}}| \tag{16}$$

$$\text{cost}_2 = Q_{\text{slack}} - Q_{\text{slack\_ref}} \tag{17}$$

$$\text{cost}_U = \text{cost}_1 \cdot K_1 + \text{cost}_2 \cdot K_2. \tag{18}$$

The active power at the slack node, P_{slack} [calculated in (19) from the voltage at node 12, *V(12)*, and the current between nodes 12 and 6, I_{12_6}], and the sum of the values of the local power at each node i (computed by combining the generated, P_{Gi}, and the consumed, P_{Li}, power) are calculated to obtain the power losses at all iterations. The cost functions, cost_3 and cost_L, associated with the objective of minimizing losses are shown in (20) and (21), where K_3 and K_4 are weighting coefficients

$$P_{\text{slack}} = \text{Real}\left(V\,(12) \times I^*_{12\_6}\right) \tag{19}$$

$$\text{cost}_3 = P_{\text{slack}} + \left(\sum_{i=1}^{n_L+n_G} P_{G_i} - P_{L_i}\right) \tag{20}$$

$$\text{cost}_L = \text{cost}_3 \cdot K_3 + \text{cost}_2 \cdot K_4. \tag{21}$$

The cost functions, cost_4, cost_5, and cost_{DF}, associated with the objective of maximizing the displacement factor are shown in (23), (25), and (26), where K_5 and K_6 are weighting coefficients. These cost functions are related to the reactive power injected from the wind farm, Q_W, and from the hot rolling mill plant, Q_{HRM}, which are calculated in (22) and (24). Node voltages, *V(1)* and *V(2)*, and currents, I_{1_7} and $I_{2\_3,}$ are used to calculate both reactive power values

$$Q_W = \text{Imag}\left(V\,(1) \times I^*_{1\_7}\right) \tag{22}$$

$$\text{cost}_4 = \text{abs}\left(Q_{WF}\right) \tag{23}$$

$$Q_{\text{HRM}} = \text{Imag}\left(V\,(2) \times I^*_{2\_3}\right) \tag{24}$$

$$\text{cost}_5 = \text{abs}\left(Q_{\text{HRM}}\right) \tag{25}$$

$$\text{cost}_{\text{DF}} = \text{cost}_4 \cdot K_6 + \text{cost}_5 \cdot K_5. \tag{26}$$

Penalties [see (27)–(30), where K_7 is a weighting coefficient], are included in such cost functions if the particle is beyond the maximum ($Q_{W_{\text{LIMIT\_MAX}}}$ for the wind farm and $Q_{\text{STAT}_{\text{LIMIT\_MAX}}}$ for the STATCOM) and minimum ($Q_{W_{\text{LIMIT\_MIN}}}$ for the wind farm and $Q_{\text{STAT}_{\text{LIMIT\_MIN}}}$ for the STATCOM)

$$\text{if } X_{1,h} > Q_{\text{W}_{\text{LIMIT\_MAX}}}$$

$$\text{penalty}_1 = K_7 + \left(X_{1,h} - \ Q_{W_{\text{LIMIT}_{\text{MAX}}}}\right) \tag{27}$$

$$\text{if } X_{1,h} < Q_{W_{\text{LIMIT\_MIN}}}$$
$$\text{penalty}_2 = K_7 + \left(-X_{1,h} + Q_{W_{\text{LIMIT}_{\text{MIN}}}}\right) \quad (28)$$
$$\text{if } X_{1,h} > Q_{\text{STAT}_{\text{LIMIT\_MAX}}}$$
$$\text{penalty}_3 = K_7 + \left(X_{1,h} - Q_{\text{STAT}_{\text{LIMIT}_{\text{MAX}}}}\right) \quad (29)$$
$$\text{if } X_{1,h} < Q_{\text{STAT}_{\text{LIMIT\_MIN}}}$$
$$\text{penalty}_4 = K_7 + \left(-X_{1,h} + Q_{\text{STAT}_{\text{LIMIT}_{\text{MIN}}}}\right). \quad (30)$$

The distribution current between two nodes $I_{i,j}$, of the network is limited by the ampacity $I_{z\_i\_j}$, of the utilized cables

$$\text{if } I_{i,j} > I_{z\_i\_j} \text{ penalty}_5 = K_7 + (I_{ij} - I_{z\_i\_j}). \quad (31)$$

The resulting cost function that the algorithm must minimize is F_x, where *x* can be *U, L,* or *DF* on the prevalent objective, see (18), (21), and (26)

$$F_x = \text{cost}_x + \sum_i \text{penalty}_i. \quad (32)$$

Based on the value of the cost functions, the best particle swarm solution (i.e., minimum value of F_x) is recorded at each iteration. An analysis of the results of the *Np* particles at the current iteration is conducted. The best results for each particle and for the whole swarm are stored.

Step 11*:* The particle position and velocity are updated. In (33) and (34), function *random* yields a random number within interval [01] and coefficient *l* can be 1 or 2

$$V_{l,h}{}^{k+1} = \omega \cdot V_{l,h}{}^{k} + c_1 \cdot \text{random} \cdot \left(p_{\text{best}\,i,h} - X_{l,h}{}^{k}\right) + c_2 \cdot \text{random} \cdot \left(G_{\text{best},i} - X_{l,h}{}^{k}\right) \quad (33)$$
$$X_{l,h}^{k+1} = X_{l,h}^{k} + V_{l,h}^{k+1}. \quad (34)$$

Step 12*:* The best reactive power references for the wind farm generators and the STATCOM are obtained after iterating for the Np particles. The STATCOM and farm reactive power references are updated every 10 ms. The optimization flowchart is shown in Fig. 11

$$\begin{bmatrix} G_{\text{best}\,1} \\ G_{\text{best}\,2} \end{bmatrix} = \begin{bmatrix} Q_W \\ Q_{\text{STAT}} \end{bmatrix}. \quad (35)$$

With regard to the three optimization objectives, the following constraints have been considered.

1) Voltage variations at nodes 3 and 8: variations must be less than 1% on 95% of the samples, which must be measured every 200 ms over 10-min periods of the average rms values.
2) Distribution network energy losses: losses must be reduced by at least 20% of those corresponding to the least demanding optimization process in this respect. Losses in the magnetic circuit of the transformers are not regarded because they are considered to be voltage-dependent, and voltage is quite stable and, therefore, minimally controllable.
3) Displacement factor at the wind farm and rolling mill PCCs to the 132-kV distribution network: this factor must be in the range 0.98 (capacitive) and 0.98 (inductive) hourly.

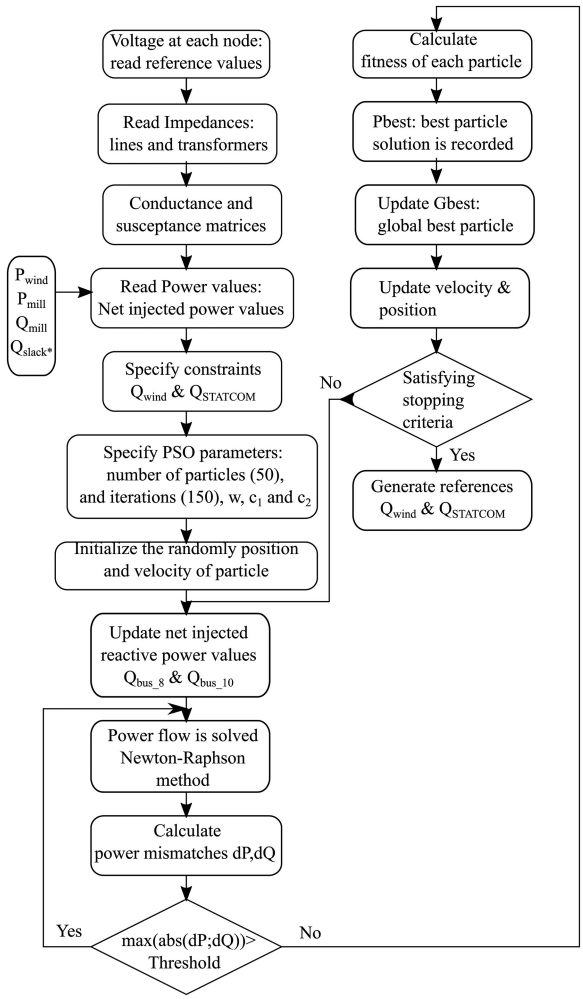

Fig. 11. Flowchart of the proposed PSO method.

The virtual plant is simulated by using general-purpose software for analyzing electrical power systems [37]. A simulation step of 5 μs is used. The optimization algorithm receives each 10 ms the input variables recorded at each of the system's measurement points (P_{HRM}, Q_{HRM}, P_{WF}). From these input variables, the algorithm determines the reactive power values that both the wind farm and the STATCOM receive as operating setpoints. The dynamic response of the various devices involved in the power flow is considered to render the obtained results meaningful. These simulations enable the verification of the fulfillment of the objectives pursued with the incorporation of the PSO strategy.

VII. Case Studies

Three case studies corresponding to the objectives described in Section V are analyzed, namely the minimization of distribution losses (case A), the maximization of the displacement factor at the 132-kV PCC of the HRM (PCC_B1; node 2) and the wind farm (PCC_B2; node 1) (case B), and the minimization

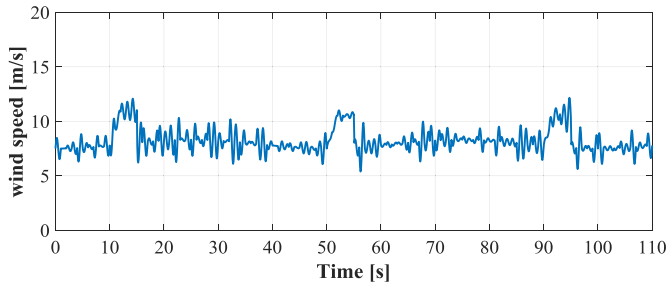

Fig. 12. Wind speed evolution over time.

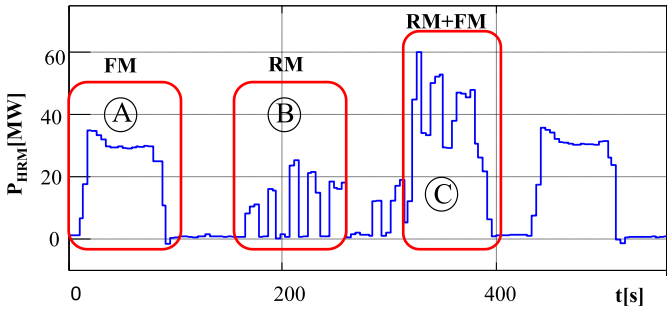

Fig. 13. Active power demanded from the HRM at different rolling stages.

of the voltage deviation at both the 690-V PCC (PCC_C1; node 8) of the turbines and the 34.5-kV PCC (PCC_C2; node 3) of the HRM (case C). The input variables of the algorithm are the active and reactive power demanded by the HRM, as well as the active power produced by the wind farm, for each case study and optimization interval. The active power generated by the waste gas recovery plant is 100 MW and its associated node voltage is 1.0045 p.u. Plant 2 behaves as a PQ load (P = 50 MW and Q = 30 Mvar).

The expected wind speed distribution during the analysis is shown in Fig. 12. This distribution comprises four fundamental components: base wind, which corresponds to the average wind speed (7.5 m/s); gust, which represents sudden wind changes; gradual wind changes, and wind of random nature.

The reactive power reference of the slack bus in cases A and C is assumed to keep constant (1.5 Mvar) according to that set by the transmission grid manager, whereas such a reference cannot be set in case B. The algorithm provides the references for the reactive power injected by the STATCOM and the wind farm. The evolution of the main variables during three rolling stages with different load profiles and dynamics is analyzed as follows. Fig. 13 shows the evolution of the active power demanded from the HRM during such stages (highlighted in red). The proper operation of the three optimization objectives is checked for the three stages.

The aforementioned rolling stages correspond to time windows:

1) between 10 and 110 s, when only the finishing mill is rolling;
2) between 173 and 263 s, when only the roughing mill is rolling,
3) between 300 and 390 s, when both the roughing and the finishing mill are simultaneously rolling one slab each.

A. Variables of Interest When Only the Finishing Mill is Rolling

The evolution of the main variables of interest when the slab is rolled in the FM is shown in Fig. 14. The wind farm produces around 9 MW according to the wind speed evolution during the analyzed period. The wind farm is forced to inject between 3 and 6 Mvar into the grid if the *loss minimization algorithm* is activated. The profile of the active and reactive power demand from the HRM is fairly homogeneous, and the entry and exit of the slab from the FM can be clearly seen as the power varies in a staggered manner. The reactive power is mostly compensated for at the rolling mill PCC to the 132-kV grid. The evolution of this reactive power is partly determined by the role played by the STATCOM together with the passive filtering system. In this stage, the optimization algorithm forces the STATCOM to provide an average of around 5 Mvar to the grid. The dynamics of the same variables can also be seen in Fig. 14 when the *voltage deviation minimization* or the *displacement factor maximization algorithms* are activated. The reactive power injected by the wind farm and the STATCOM is adapted to the needs of each optimization target.

Fig. 15 (left) shows the evolution of the distribution losses for each case study (LS: minimization of losses; DF: maximization of displacement factor; AU: minimization of voltage deviation). As can be seen, the maximum difference (roughly 400 kW) occurs between cases A (2 MW) and B (2.4 MW) when the FM is loaded. On another note, the iron losses of the network transformers are expected to be 864 kW. These losses can be considered practically constant given the small variation observed in the voltage of the transformers PCC.

Therefore, 400 kW in case A represent 26% of the total losses that can be controlled (2.4 MW – 864 kW = 1.536 MW), which is a significant benefit. In the same figure, voltage variations at the monitored nodes, PCC_C1 (corresponding to the wind farm, WF) and PCC_C2 (associated with the HRM) can be seen. With regard to the voltage at PCC_C1 and PCC_C2, their optimum references are set to 1 and 1.05 p.u., respectively (note that these references do not have necessarily to be 1 p.u.). Maximum voltage variations with respect to the optimum value are always of the order of 1% (when the algorithm optimizes voltage variations, the voltages are adjusted to their reference, but the dynamics of the power devices involved generate small variations that are observed in the records).

B. Evolution of the Main Variables During Rolling in the Roughing Mill

The evolution of the main variables of interest when one slab is rolled in the RM is shown in Fig. 16 (cases A, B, and C). In this case, the distinct variations in the evolution of the active and reactive power clearly reflect the five passes that the slab is subjected to. The analysis of the results obtained for these rolling circumstances and under the three optimization algorithms is performed by comparing the distribution network losses and the

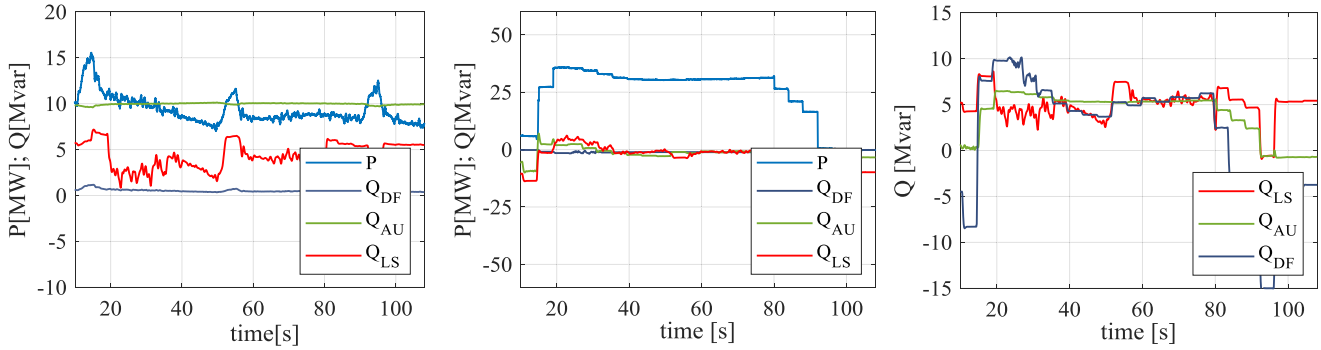

Fig. 14. Cases A, B, and C when a slab is rolled in the FM. From left to right: 1) Active (blue) and reactive (red, green, dark blue) power injected by the wind farm. 2) Active (blue) and reactive (red, green, dark blue) power demanded by the HRM at PCC_B1(node 2). 3) Reactive power injected by the STATCOM.

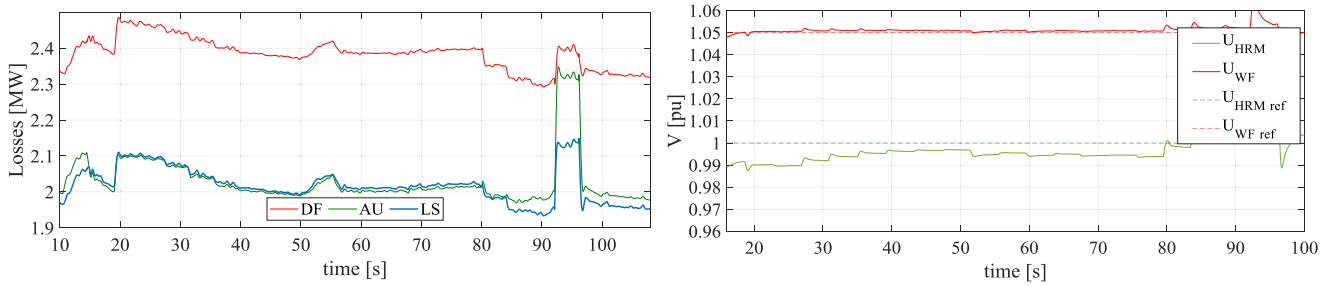

Fig. 15. Evolution of losses (left) for the three optimization algorithms and of the voltage at PCC_C1 and PCC_C2 (right) for the algorithm to minimize voltage deviations.

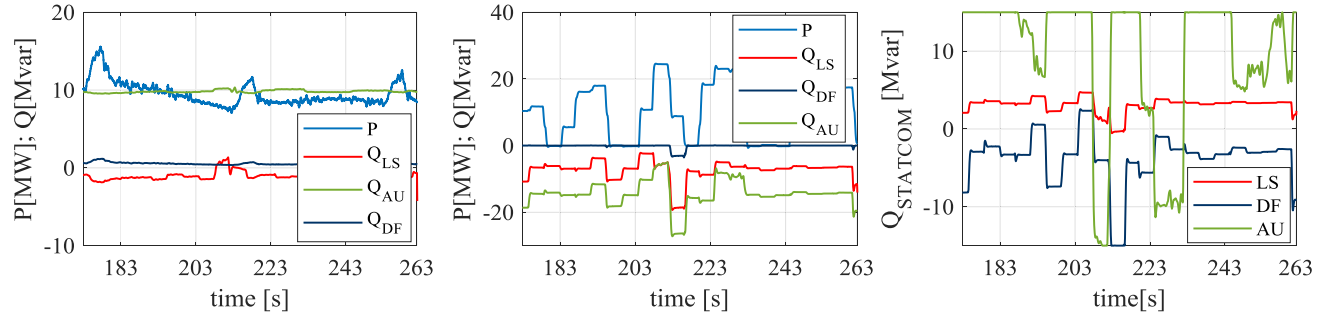

Fig. 16. Cases A, B, and C when a slab is rolled in the RM. From left to right: 1) Active (blue) and reactive (red, green, dark blue) power injected by the wind farm. 2) Active (blue) and reactive (red, green, dark blue) power demanded by the HRM at PCC_B1(node 2). 3) Reactive power injected by the STATCOM.

voltage variations (see Fig. 17) at the monitored nodes, PCC_C1 and PCC_C2.

C. Evolution of the Main Variables During Rolling Simultaneously in the Roughing and Finishing Mill

On the other hand, the evolution of the same variables when two slabs are rolled simultaneously, one in the RM and the other in the FM, is plotted in Fig. 18 (cases A, B, and C).

The analysis of the results obtained for these rolling circumstances and under the three optimization algorithms is performed by comparing the distribution network losses. The voltage variations at the monitored nodes are also shown for the algorithm to the minimize voltage deviations (see Fig. 19).

D. Summary

Tables V– VII summarize the comparative analysis of losses, voltage deviations and displacement factors obtained when using each of the three algorithms (LS, DF and AU), three rolling circumstances (when a slab is rolled in the FM or in the RM, and when two slabs are rolled simultaneously in the RM and in the FM), and two monitored nodes (PCC_C1 and PCC_C2).

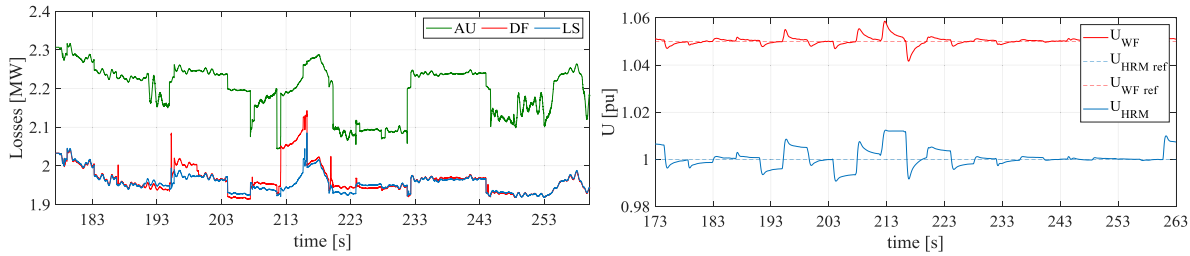

Fig. 17. Evolution of losses when a slab is rolled in the RM (left) and of the voltage at PCC_C1 and PCC_C2 (right) for the algorithm to minimize voltage deviations.

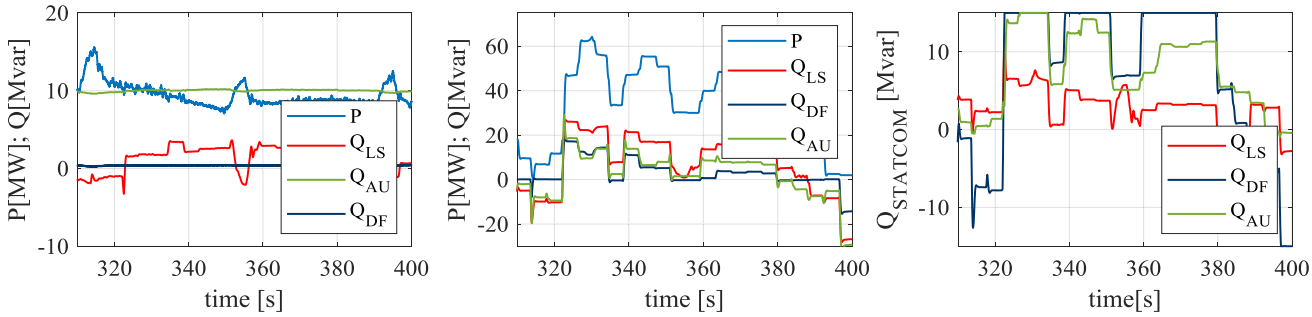

Fig. 18. Cases A, B, and C when two slabs are rolled simultaneously in the RM and the FM. From left to right: 1) Active (blue) and reactive (red, green, dark blue) power injected by the wind farm. 2) Active (blue) and reactive (red, green, dark blue) power demanded by the HRM at PCC_B1(node 2). 3) Reactive power injected by the STATCOM.

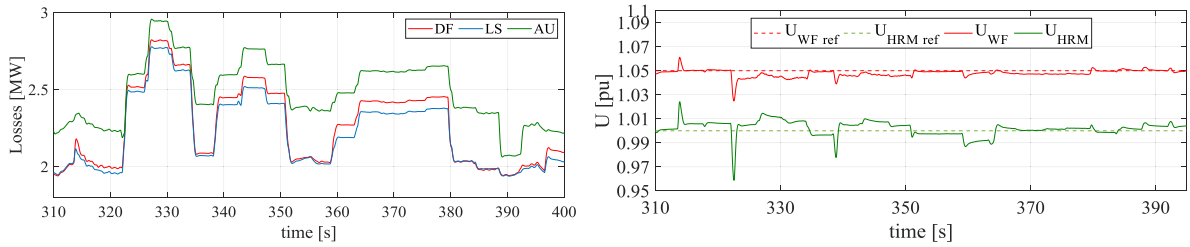

Fig. 19. Evolution of losses (left) for the three optimization algorithms and of the voltage at PCC_C1 and PCC_C2 (right) for the algorithm to minimize voltage deviations when two slabs are rolled simultaneously in the RM and the FM.

TABLE V
COMPARATIVE ANALYSIS OF ENERGY LOSSES

	Rolling process									
	Finishing Mill			Roughing Mill			Finishing mill & Roughing Mill			Global
Optimization target	Energy losses[kWh]	Savings [%]	Savings [%]**	Energy losses[kWh]	Savings [%]	Savings [%]**	Energy losses[kWh]	Savings [%]	Savings [%]**	Savings [%]**
AU*	70.8	0	0	67.5	0	0	74.5	0	0	0
DF	61.5	2.7	4.84	60.4	0.8	1.4	67.5	9.4	14.5	3
LS	59.8	**15.5**	**24.7**	59.9	**2.7**	**4.8**	66.5	**10.7**	**16.6**	**20%**

Note: * least efficiency case; **: deducting transformer energy losses.

More specifically, the maximum voltage deviation that occurs is indicated for each case.

If the three rolling stages are considered in a global manner, losses are reduced by 12.5% when adopting the losses minimization strategy in comparison to the least efficient case, as seen in Table V, where the values for each rolling stage correspond to 100 s intervals. The global savings are 20% if energy losses in transformers are deducted based on their being incontrollable. An average saving of 130 kWh is achieved when rolling 10 slabs if such a strategy is employed, which yields savings of 6.5 MWh per day and 2.3 GWh per year assuming a daily rolling rate of 500 slabs. Voltage variations are maintained at less than

TABLE VI
COMPARATIVE ANALYSIS OF MAXIMUM VOLTAGE DEVIATION

	Rolling process					
	Finishing Mill		Roughing Mill		Finishing mill & Roughing Mill	
Optimization target	AU PCC_C1 [%]	PCC_C2 [%]	PCC_C1 [%]	PCC_C2 [%]	PCC_C1 [%]	PCC_C2 [%]
AU	**1**	**1**	**1**	**1**	**1**	**1**
DF	2.5	4	1	4	3	4
LS	4	2	4	2.7	4	5

TABLE VII
COMPARATIVE ANALYSIS OF DISPLACEMENT FACTOR

	Rolling process					
	Finishing Mill		Roughing Mill		Finishing mill & Roughing Mill	
Optimization target	DF HRM	DF WF	DF HRM	DF WF	DF HRM	DF WF
AU	0.99	0.7	0.85	0.7	0.98	0.95
DF	**1**	**1**	**1**	**1**	**1**	**1**
LS	0.9	0.91	0.85	0.9	0.98	0.99

1% at both nodes when employing the strategy for minimizing voltage deviations, whereas fluctuations between 1% and 5% are reached when implementing the other two strategies, as seen in Table VI. The displacement factor is kept close to unity at nodes 1 and 2 if the strategy for maximizing the displacement factor is selected. On the contrary, the displacement factor at these nodes can reach notably poor values when the other strategies are adopted, especially at node 2, as shown in Table VII.

The quality of the solution is particularly simple to assess when optimizing the displacement factor or minimizing the voltage variations. In these cases, a small margin for improvement can be observed. If the target is the minimization of losses, the upper and lower limits make it possible to verify that the solution is within the optimal range, the former limit being obtained when other objectives are pursued, and the latter being set by the no-load transformer losses.

VIII. VALIDATION OF RESULTS

The utilized PSO algorithm is able to give a response within an optimal range in a reasonably short time (10 ms), which perfectly suits the demanding dynamics of the steel plant. Moreover, the computational cost associated with this algorithm is low. Furthermore, its flexibility is greater than that of more reliable and robust linear programming-based methods, thus making it able to work with both linear systems and nonlinearities such as those associated with the responses produced by the wind farm and the STATCOM themselves. Although optimization strategies based on genetic algorithms also deliver good performance under non-linear constraints, their computational cost is higher [38].

The results obtained by applying the PSO algorithm have been compared with those yielded by the Matlab function called *fmincon* [39], [40]. This function finds a minimum value of a constrained nonlinear multivariable function. It is an interior-point optimization algorithm and a nonlinear programming solver. In particular, the comparison is made when the LS algorithm is selected, as is the case for which the validity of the results can be more uncertain. The syntax of the function would be

$$[a,b] = \boldsymbol{fmincon}(@\text{MinLoss}, x0, [],[], [],[], xlb\,(P\_\text{wind}), xub\,(P\_\text{wind}), @\text{Qslack\_cal}, \text{options}) \tag{36}$$

where

- a is a vector including the two control variables that enable the optimization, *a(1)* being the reactive power injected by the wind farm and *a(2)* standing for that provided by the STATCOM;
- b represents the overall system losses to be minimized;
- @MinLoss is the call for the m-file regarding the multivariable function to minimize, which is described in Section VI, see (21) and (32). Prior to the cost assessment, it is necessary to solve a load flow with the forecasts made by *fmincon* for the reactive power injection from both the wind farm and the STATCOM;
- *x0* is the initial guess;
- the spaces between square brackets *[]* correspond to the linear inequality and equality constraints, which are not considered in this case;
- *xlb* and *xub* are the lower and upper bounds, which depend on the active power of the wind farm, *P*_wind;
- @*Q*slack_cal is the call for the m-file regarding the nonlinear constraints. The reactive power in the slack node, $Q_{\text{slack}}*$, must be adapted to the reference set by the grid operator.

Fig. 20 shows the evolution of the main input variables (P_{HRM}, Q_{HRM}, P_{WF}) which are the same for both the PSO algorithm and the *fmincon* function, as is the slack bus reactive power reference ($Q_{\text{slack}}* = 1.5$ Mvar). Fig. 21 shows the evolution of the primary output control variables, i.e., the reactive power references for the wind farm and the STATCOM. The accordance between the results yielded by both methods can

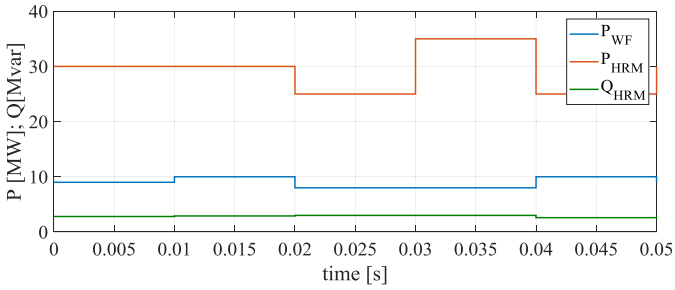

Fig. 20. Evolution of the main input variables during the comparative analysis.

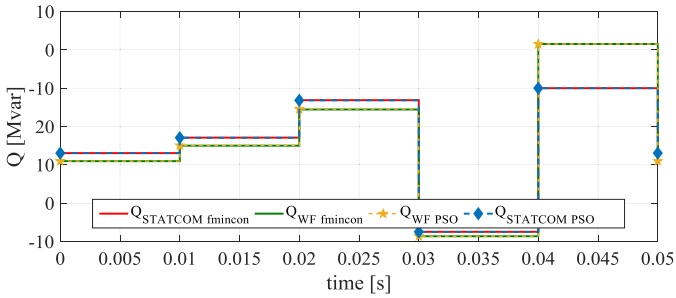

Fig. 21. Evolution of the main control variables during the comparative analysis.

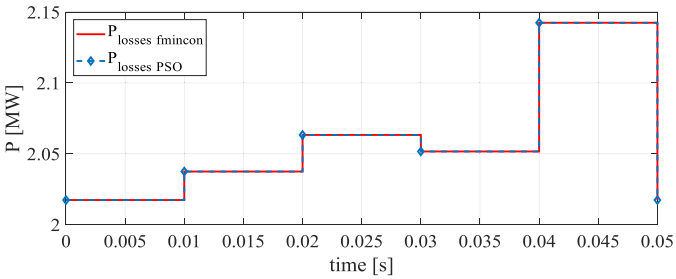

Fig. 22. Evolution of the distribution losses during the comparative analysis.

be noticed. Meanwhile, Fig. 22 shows the evolution of the distribution network losses when calculated with each of the optimization methods. The total agreement of the results can be observed. Despite obtaining the same results, the PSO algorithm has various advantages over *fmincon*: 1) separate cores of a single computer can be used to run different particles of the PSO algorithm simultaneously, which renders this technique much faster; 2) the PSO algorithm is more flexible than *fmincon*, and 3) the PSO algorithm supports different optimization targets that can be weighted and processed in parallel.

Moreover, Fig. 23 shows the evolution of both the main control variables and the losses during the analysis made in section VII.A that is represented in Fig. 14.

The results obtained with the PSO-based algorithm when a real dynamic variation of the input variables occurs are compared with those obtained with *fmincon*. The coincidence of the results can be observed, which supports the validity of the proposed method and the obtained results.

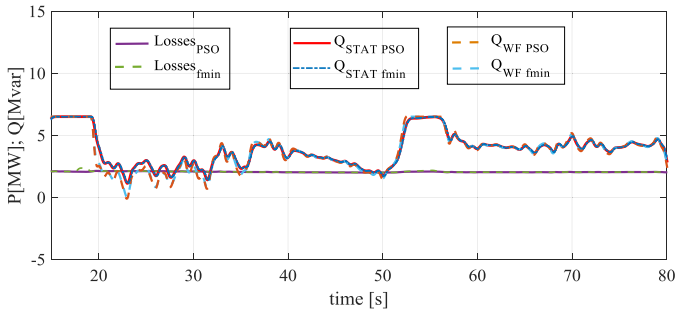

Fig. 23. Evolution of the distribution losses and main output control variables during the comparative analysis.

IX. Conclusion

The opportunities offered by a collaborative operation of steel plants and power generation centers have been analyzed in this paper. The specific proposal consists in integrating a wind farm and a steelmaking factory into a virtual plant managed by a single operator. Special attention has been paid to the optimal management of reactive power, which has been solved by using the so-called particle swarm optimization. This method can address different objective functions. Accordingly, optimization of losses, of two node voltages and of the displacement factor have been assessed. The obtained results demonstrate the advantages of the coordinated management of energy and the effectiveness of the utilized optimization algorithm.

References

[1] European Union Publications, Brussels, Belgium, "Towards competitive and clean European steel," Commission Staff Working Document 5.5.2021 SWD (2021) 353 final, 2021.

[2] F. Delfino, G. Ferro, M. Robba, and M. Rossi, "An energy management platform for the optimal control of active and reactive powers in sustainable microgrids," *IEEE Trans. Ind. Appl.*, vol. 55, no. 6, pp. 7146–7156, Nov./Dec. 2019.

[3] R. Zhang and B. Hredzak, "Distributed dynamic clustering algorithm for formation of heterogeneous virtual power plants based on power requirements," *IEEE Trans. Smart Grid*, vol. 12, no. 1, pp. 192–204, Jan. 2021.

[4] Z. Tan, H. Zhong, Q. Xia, C. Kang, X. S. Wang, and H. Tang, "Estimating the robust P-Q capability of a technical virtual power plant under uncertainties," *IEEE Trans. Power Syst.*, vol. 35, no. 6, pp. 4285–4296, Nov. 2020.

[5] J. García-González, J. L. Luis Mata, and R. Veguillas, "Improving the integration of renewable sources in the european electricity networks," in *Proc. IEEE PES Gen. Meeting*, 2010, pp. 1–2, doi: 10.1109/PES.2010.5589567.

[6] A. Mnatsakanyan and S. W. Kennedy, "A novel demand response model with an application for a virtual power plant," *IEEE Trans. Smart Grid*, vol. 6, no. 1, pp. 230–237, Jan. 2015.

[7] A. Thavlov and H. W. Bindner, "Utilization of flexible demand in a virtual power plant set-up," *IEEE Trans. Smart Grid*, vol. 6, no. 2, pp. 640–647, Mar. 2015.

[8] M. Vasirani, R. Kota, R. L. G. Cavalcante, S. Ossowski, and N. R. Jennings, "An Agent-based approach to virtual power plants of wind power generators and electric vehicles," *IEEE Trans. Smart Grid*, vol. 4, no. 3, pp. 1314–1322, Sep. 2013,.

[9] G. A. Orcajo, J. M. Cano, J. G. Norniella, F. Pedrayes González, C. H. Rojas, and D. Josué Rodríguez, "Coordinated management of electrical energy in a hot rolling mill and a wind farm," in *Proc. IEEE Ind. Appl. Soc. Annu. Meeting*, Oct. 2021, pp. 1–9.

[10] T. Ding, S. Liu, W. Yuan, Z. Bie, and B. Zeng, "A two-stage robust reactive power optimization considering uncertain wind power integration in active distribution networks," *IEEE Trans. Sustain. Energy*, vol. 7, no. 1, pp. 301–311, Jan. 2016.

[11] O. Alsac, J. Bright, M. Prais, and B. Stott, "Further developments in Lp-based optimal power flow," *IEEE Trans. Power Syst.*, vol. 5, no. 3, pp. 697–711, Aug. 1990.
[12] M. B. Liu, S. K. Tso, and Y. Cheng, "An extended nonlinear primal-dual interior-point algorithm for reactive-power optimization of large-scale power systems with discrete control variables," *IEEE Trans. Power Syst.*, vol. 17, no. 4, pp. 982–991, Nov. 2002.
[13] J. Z. Zhu, C. S. Chang, W. Yan, and G. Y. Xu, "Reactive power optimization using an analytic hierarchical process and a nonlinear optimization neural network approach," *IEE Proc. Gener., Transmiss., Distrib.*, vol. 145, pp. 89–97, 1998.
[14] K. Iba, "Reactive power optimization by genetic algorithm," *IEEE Trans. Power Syst.*, vol. 9, no. 2, pp. 685–692, May 1994.
[15] S. H. Zanakis and J. R. Evans, "Heuristics optimization: Why, When and How to use it," *Interfaces*, vol. 11, no. 5, pp. 84–91, Oct. 1981.
[16] B. Zhao, C. X. Guo, and Y. J. Cao, "A multiagent-based particle swarm optimization approach for optimal reactive power dispatch," *IEEE Trans. Power Syst.*, vol. 20, no. 2, pp. 1070–1078, May 2005.
[17] H. Yoshida *et al.*, "A particle swarm optimization for reactive power and voltage control considering voltage security assessment," *IEEE Trans. Power Syst.*, vol. 15, no. 4, pp. 1232–1239, Nov. 2000.
[18] D. Koraki and K. Strunz, "Wind and solar power integration in electricity markets and distribution networks through service-centric virtual power plants," *IEEE Trans. Power Syst.*, vol. 33, no. 1, pp. 473–485, Jan. 2018.
[19] G. A. Orcajo *et al.*, "Dynamic estimation of electrical demand in hot rolling mills," *IEEE Trans. Ind. Appl.*, vol. 52, no. 3, pp. 2714–2736, May/Jun. 2016.
[20] Y. Zhang, E. Muljadi, D. Kosterev, and M. Singh, "Wind power plant model validation using synchrophasor measurements at the point of interconnection," *IEEE Trans. Sustain. Energy*, vol. 6, no. 3, pp. 984–992, Jul. 2015.
[21] R. Cardenas, R. Pena, S. Alepuz, and G. Asher, "Overview of control systems for the operation of DFIGs in wind energy applications," *IEEE Trans. Ind. Electron.*, vol. 60, no. 7, pp. 2776–2798, Jul. 2013.
[22] L. Yang, Z. Xu, J. Ostergaard, Z. Y. Dong, and K. P. Wong, "Advanced control strategy of DFIG wind turbines for power system fault ride through," *IEEE Trans. Power Syst.*, vol. 27, no. 2, pp. 713–722, May 2012.
[23] ArcelorMittal News, "Storm is building Belgium's first subsidy-free wind farm at ArcelorMittal Belgium in Ghent." 2022. Accessed: Dec. 3, 2021. [Online]. Available: https://Belgium.arcelormittal.com/en/storm-is-building-belgiums-first-subsidy-free-wind-farm-on-the-grounds-of-arcelormittal-Belgium-in-ghent/
[24] F.-A. Bourhim, S. Berrhazi1, A. Ouammi, and R. Benchrifa, "Decision support model for optimal design of wind technologies based techno–economic approach," *IEEE Access*, vol. 9, pp. 148264–148276, 2021.
[25] J. V. Milanovic and Y. Zhang, "Global minimization of financial losses due to voltage sags with FACTS based devices," *IEEE Trans. Power Del.*, vol. 25, no. 1, pp. 298–306, Jan. 2010.
[26] Daily Carbon Prices. Accessed: Mar. 3, 2022. [Online]. Available: https://ember-climate.org/data/carbon-price-viewer//
[27] A. Giannitrapani, S. Paoletti, A. Vicino, and D. Zarrilli, "Bidding wind energy exploiting wind speed forecasts," *IEEE Trans. Power Syst.*, vol. 31, no. 4, pp. 2647–2656, Jul. 2016.
[28] D. Jager and A. Andreas, "NREL national wind technology center (NWTC): M2 tower," NREL, Boulder, CO, USA, Rep. DA-5500-56489, 1996, doi: 10.5439/1052222.
[29] R. Dones, T. Heck, and S. Hirschberg, "Greenhouse gas emissions from energy systems, comparison and overview," *Encyclopedia Energy*, vol. 3, pp. 77–95, 2004, doi: 10.1016/B0-12-176480-X/00397-1.
[30] M. A. Martínez, "Gestión óptima de potencia reactiva en sistemas eléctricos con generación eólica," Ph.D. dissertation, Carlos III Univ., Leganés, Spain, 2010.
[31] T. Lund, P. Sorensen, and J. Eek, "Reactive power capability of a wind turbine with doubly fed induction generator," *Wind Energy*, vol. 10, pp. 379–394, 2007.
[32] Spanish Regulation, BOE-A-2014-6123 Real Decreto 413/2014. Jun. 2014. [Online]. Available: https://www.boe.es/diario_boe/txt.php?id=BOE-A-2014-6123
[33] S. I. Deaconu, G. N. Popa, and R. Babău, "Study, design and industrial implementation of capacitive power factor controller for large load fluctuations in steel industry," in *Proc. Int. Conf. Expo. Elect. Power Eng.*, 2014, pp. 962–967, doi: 10.1109/ICEPE.2014.6970052.
[34] Y. L. Chen and C. C. Liu, "Optimal multi-objective Var planning using an interactive satisfying method," *IEEE Trans. Power Syst.*, vol. 10, no. 2, pp. 664–670, May 1995.
[35] M. Eghbal, N. Yorino, E. E. El-Arabi, and Y. Zoka, "Multi-load level reactive power planning considering slow and fast VAR devices by means of particle swarm optimization," *IET Gener. Transmiss. Distrib.*, vol. 2, no. 5. pp. 743–751, 2008.
[36] J. M. Cano, J. G. Norniella, C. H. Rojas, G. A. Orcajo, and J. Jatskevich, "Application of loop power flow controllers for power demand optimization at industrial customer sites," in *Proc. IEEE Power Energy Soc. Gen. Meeting*, 2015, pp. 1–5.
[37] MathWorks, "The MathWorks—MATLAB and Simulink for technical computing," 2021. [Online]. Available: http://www.mathworks.com
[38] P. Hou, W. Hu, M. Soltani, and Z. Chen, "Optimized placement of wind turbines in large-scale offshore wind farm using particle swarm optimization algorithm," *IEEE Trans. Sustain. Energy*, vol. 6, no. 4, pp. 1272–1282, Oct. 2015.
[39] B. Kanna and S. N. Singh, "Towards reactive power dispatch within a wind farm using hybrid PSO," *Elect. Power Energy Syst.*, vol. 69. pp. 232–240, , 2015.
[40] A. H. Khan *et al.*, "Optimal portfolio management for engineering problems using Nonconvex Cardinality constraint: A computing perspective," *IEEE Access*, vol. 8, pp. 57437–57450, 2020.

Gonzalo Alonso Orcajo (Member, IEEE) was born in Gijón, Spain, in 1965. He received the M.Sc. and Ph.D. degrees in electrical engineering from the University of Oviedo, Gijón, Spain, in 1990 and 1998, respectively.

In 1992, he joined the Department of Electrical Engineering, University of Oviedo, where he is currently an Associate Professor. His main research interests include the field of power quality in industrial power systems. In recent years, he has focused on the detection and location of faults in distribution systems and on reactive power compensation systems.

Josué Rodríguez Diez was born in Pravia, Spain, in 1989. He received the M.Sc. degree in electrical engineering in 2014 from the University of Oviedo, Gijón, Spain, where he is currently working toward the Ph.D. degree in electrical engineering.

He currently works with ArcelorMittal Global R&D. He is focusing in EAF, raw material characterization, automatize and digitalization topics. He was a Research Fellow with the Department of Electrical Engineering, University of Oviedo. During 2 years, he joined the Department of Beams Radio Frequency Power Amplifiers, CERN, Switzerland. His research interests include the field of reactive power compensation systems and power quality.

José M. Cano (Senior Member, IEEE) received the M.Sc. and Ph.D. degrees in electrical engineering from the University of Oviedo, Gijón, Spain, in 1996 and 2000, respectively.

In 1996, he joined the Department of Electrical Engineering, University of Oviedo, where he is currently a Full Professor. During 2012 and 2014, he was a Visiting Associate Professor with the Department of Electrical and Computing Engineering, University of British Columbia, Canada. His main research interests include power quality solutions for industry, power converters, power system state estimation, distributed generation, and smart grids.

Joaquín G. Norniella was born in Gijón, Spain, in 1980. He received the M.Sc. and Ph.D. degrees in electrical engineering from the University of Oviedo, Gijón, Spain, in 2005 and 2012, respectively.

He worked as a Research and Development Engineer with the Department of Electronic Engineering, University of Oviedo, for 20 months since February 2007. In 2008, he joined the Department of Electrical Engineering, University of Oviedo, where he is currently working as an Associate Professor. His main research interests include the field of power quality solutions for industry and power converters.

Joaquín Francisco Pedrayes González was born in Gijón, Spain, in 1973. He received the M.Sc. and Ph.D. degrees in electrical engineering from the University of Oviedo, Gijón, Spain, in 2001 and 2007, respectively.

He is currently working as an Assistant Professor with the University of Oviedo.

Carlos H. Rojas was born in Caracas, Venezuela, in 1969. He received the electrical engineering degree from the Simón Bolivar University, Caracas, in 1994, and the Ph.D. degree in electrical engineering from the University of Oviedo, Gijón, Spain, in 2001.

He is currently an Associate Professor with the University of Oviedo. His main research interests include the field of FEM modeling of electrical machines, predictive maintenance of electrical equipment, and power quality in industrial power systems.